Stochastic numerical technique for solving HIV infection model of CD4+ T cells

Muhammad Umar[1, a], Zulqurnain Sabir[1, b], Fazli Amin[1, c], Juan L.G. Guirao[2, d, *], Muhammad Asif Zahoor Raja[3, e]

[1]Department of Mathematics and Statistics, Hazara University, Mansehra, Pakistan

[a]Email: umar_maths@hu.edu.pk,

[b]Email: zulqurnain_maths@hu.edu.pk

[c]Email: fazliamin@hu.edu.pk

[2]Department of Applied Mathematics and Statistics, Technical University of Cartagena, Hospital de Marina 30203-Cartagena, Spain

[d]Email: juan.garcia@upct.es

[3]Department of Electrical and Computer Engineering, COMSATS University Islamabad, Attock Campus, Attock 43600, Pakistan

[e]Email: muhammad.asif@ciit-attock.edu.pk

Abstract: The intension of the present work is to present the stochastic numerical approach for solving Human Immunodeficiency Virus (HIV) infection model of cluster of differentiation 4 of T-cells, i.e., CD4+ T cells. A reliable integrated intelligent computing framework using layered structure of neural network with different neurons and their optimization with efficacy of global search by genetic algorithms (GAs) supported with rapid local search methodology of active-set method, i.e., hybrid of GA-ASM, is used for solving the HIV infection model of CD4+ T cells. A comparison between the present results for different neurons based models and the numerical values of the Runge-Kutta method reveals that the present intelligent computing techniques is trustworthy, convergent and robust. Statistics based observation on different performance indices further demonstrates the applicability, effectiveness and convergence of the present schemes.

Keywords: HIV infection, genetic algorithms, hybrid approach, sequential quadratic programming, artificial neural networks, statistical analysis.

1. Introduction

In recent years, numerous mathematical models have been built-up for human immunodeficiency virus (HIV) infectious dynamics of cluster of differentiation 4 of T-cells, i.e., CD4+ T cells. The present study is about the HIV infection model [1]. This model is the combination of three basic component models, which are CD4+ T cells septic by the HIV viruses, attention of susceptible cells and free HIV virus elements in the blood. The general form of the model is a system of three nonlinear system of differential equations, written as [1]:

$$\begin{cases} \dfrac{dT}{dt} = rT\left(1-\dfrac{T+I}{T_{\max}}\right)-\alpha T+q-kVT, & T(0)=r_1, \\ \dfrac{dI}{dt} = -\beta I+kVT, & I(0)=r_2, \\ \dfrac{dV}{dt} = -\gamma V+n\beta I, & V(0)=r_3, \end{cases} \tag{1}$$

where $T(t)$, $I(t)$ and $V(t)$ represent the concentration of CD4+ T cells, septic from the viruses of HIV and virus free particles, respectively. Furthermore, r, $T_{\max}$, q, k and n respectively denote growth rate of CD4+ T cell concentration, maximal attention of CD4+ T cells, source factor due to uninfected CD4+T cells, the virus infected rate of CD4+T cells and virus particles created by each infected CD4+T cell. While, α, β and γ are the natural death rate of uninfected CD4+T cells, infected CD4+T cells and virus free particles, respectively.

Recently, many numerical techniques have been presented to solve the HIV infection spread model given in equation (1) [1-7]. These numerical procedures have their individual advantages and drawbacks, whereas, stochastic numerical solvers based on artificial neural networks (ANNs) are looks promising to be exploited for HIV infection spread and control models due to their ability of accurate modeling, precision, consistency and efficiency for solving optimization problems arising in various fields [8-12]. Recent applications of stochastic solvers are nonlinear Troesch's problem [13], inverse kinematics problems [14], cell biology [15], nonlinear prey-predator models [16], power [17], thin film flow [18], fuzzy differential equations [19], uncertainties in computational mechanics [20], nonlinear singular Thomas-Fermi systems [21], nanofluidics problems [22], heat conduction model of human head [23], nonlinear optics [24], doubly-singular systems [25], control autoregressive moving average systems [26], transistor-level uncertainty quantification [27] and energy [28].

The intension of the present work is to solve the model (1) numerically using the ANNs optimized by genetic algorithm (GA), active-set method (ASM) and the hybrid of GA-ASM. The reliability and exactness is checked by comparing the present results with the Runge-Kutta (RK) numerical scheme. Furthermore, the accuracy of the present scheme evaluated through statistical analysis.

2. Design Methodology

The design methodology of the present scheme is divided in two parts for numerical solution of HIV model (1). In part 1, we introduce an error based fitness function, while in part 2, the combination of GA with ASM, i.e., GA-SQP optimization scheme is given in means of introductory material, applications, pseudocode and flow charts. The graphical abstract of the methodology is presented in Fig. 1.

2.1 ANN Modeling

The model (1) is formulated with feed-forward layer structure of ANNs, i.e., single input, hidden and output layers, to approximate the $T(t)$, $I(t)$ and $V(t)$, as well as, their respective derivatives of order n as:

$$\left[\hat{T}(t),\hat{I}(t),\hat{V}(t)\right]=\left[\sum_{i=1}^{m}\varphi_{T,i}h(w_{T,i}t+b_{T,i}),\ \sum_{i=1}^{m}\varphi_{I,i}h(w_{I,i}t+b_{I,i}),\sum_{i=1}^{m}\varphi_{V,i}h(w_{V,i}t+b_{V,i})\right],$$

$$\left[\hat{T}^{(n)},\hat{I}^{(n)},\ \hat{V}^{(n)}\right]=\left[\sum_{i=1}^{m}\varphi_{T,i}h^{(n)}(w_{T,i}t+b_{T,i}),\ \sum_{i=1}^{m}\varphi_{I,i}h^{(n)}(I_{I,i}t+b_{I,i}),\sum_{i=1}^{m}\varphi_{V,i}h^{(n)}(I_{V,i}t+b_{V,i})\right], \quad (2)$$

for m neurons, while the weight vector $\boldsymbol{W}$ is defined as:

$\boldsymbol{W}=[\boldsymbol{W}_T,\boldsymbol{W}_I,\boldsymbol{W}_V]$, for $\boldsymbol{W}_T=[\boldsymbol{\varphi}_T,\boldsymbol{w}_T,\boldsymbol{b}_T]$, $\boldsymbol{W}_I=[\boldsymbol{\varphi}_I,\boldsymbol{w}_I,\boldsymbol{b}_I]$ and $\boldsymbol{W}_V=[\boldsymbol{\varphi}_V,\boldsymbol{w}_V,\boldsymbol{b}_V]$. The components of weight vector $\boldsymbol{W}$ are given as:

$\boldsymbol{\varphi}_T = [\varphi_{T,1}, \varphi_{T,2}, \varphi_{T,3}, ..., \varphi_{T,m}]$, $\boldsymbol{\varphi}_I = [\varphi_{I,1}, \varphi_{I,2}, \varphi_{I,3}, ..., \varphi_{I,m}]$, $\boldsymbol{\varphi}_V = [\varphi_{V,1}, \varphi_{V,2}, \varphi_{V,3}, ..., \varphi_{V,m}]$,
$\boldsymbol{w}_T = [w_{T,1}, w_{T,2}, w_{T,3}, ..., w_{T,m}]$, $\boldsymbol{w}_I = [w_{I,1}, w_{I,2}, w_{I,3}, ..., w_{I,m}]$, $\boldsymbol{w}_V = [w_{V,1}, w_{V,2}, w_{V,3}, ..., w_{V,m}]$,
$\boldsymbol{b}_T = [b_{T,1}, b_{T,2}, b_{T,3}, ..., b_{T,m}]$, $\boldsymbol{b}_I = [b_{I,1}, b_{I,2}, b_{I,3}, ..., b_{I,m}]$, and $\boldsymbol{b}_V = [b_{V,1}, b_{V,2}, b_{V,3}, ..., b_{V,m}]$.

The networks (2) up to second order, i.e., $n = 2$, using the log-sigmoid activation function $1/(1+\exp(-t))$ are written, respectively, as:

$$\left[\hat{T}(t), \hat{I}(t), \hat{V}(t)\right] = \left[\sum_{i=1}^{m} \frac{\varphi_{T,i}}{1+e^{-\left(w_{T,i}t+b_{T,i}\right)}}, \sum_{i=1}^{m} \frac{\varphi_{I,i}}{1+e^{-\left(w_{I,i}t+b_{I,i}\right)}}, \sum_{i=1}^{m} \frac{\varphi_{V,i}}{1+e^{-\left(w_{V,i}t+b_{V,i}\right)}}\right],$$

$$\left[\hat{T}'(t), \hat{I}'(t), \hat{V}'(t)\right] = \left[\sum_{i=1}^{m} \frac{\varphi_{T,i} w_{T,i} e^{-\left(w_{T,i}t+b_{T,i}\right)}}{\left(1+e^{-\left(w_{T,i}t+b_{T,i}\right)}\right)^2}, \sum_{i=1}^{m} \frac{\varphi_{I,i} w_{I,i} e^{-\left(w_{I,i}t+b_{I,i}\right)}}{\left(1+e^{-\left(w_{I,i}t+b_{I,i}\right)}\right)^2}, \sum_{i=1}^{m} \frac{\varphi_{V,i} w_{V,i} e^{-\left(w_{V,i}t+b_{V,i}\right)}}{\left(1+e^{-\left(w_{V,i}t+b_{V,i}\right)}\right)^2}\right],$$

$$\left[\hat{T}''(t), \hat{I}''(t), \hat{V}''(t)\right] = \left[\begin{array}{l} \displaystyle\sum_{i=1}^{m} \varphi_{T,i} w_{T,i}^2 \left\{\frac{2e^{-2\left(w_{T,i}t+b_{T,i}\right)}}{\left(1+e^{-\left(w_{T,i}t+b_{T,i}\right)}\right)^3} - \frac{e^{-\left(w_{T,i}t+b_{T,i}\right)}}{\left(1+e^{-\left(w_{T,i}t+b_{T,i}\right)}\right)^2}\right\}, \\ \displaystyle\sum_{i=1}^{m} \varphi_{I,i} w_{I,i}^2 \left\{\frac{2e^{-2\left(w_{I,i}t+b_{I,i}\right)}}{\left(1+e^{-\left(w_{I,i}t+b_{I,i}\right)}\right)^3} - \frac{e^{-\left(w_{I,i}t+b_{I,i}\right)}}{\left(1+e^{-\left(w_{I,i}t+b_{I,i}\right)}\right)^2}\right\}, \\ \displaystyle\sum_{i=1}^{m} \varphi_{V,i} w_{V,i}^2 \left\{\frac{2e^{-2\left(w_{V,i}t+b_{V,i}\right)}}{\left(1+e^{-\left(w_{V,i}t+b_{V,i}\right)}\right)^3} - \frac{e^{-\left(w_{V,i}t+b_{V,i}\right)}}{\left(1+e^{-\left(w_{V,i}t+b_{V,i}\right)}\right)^2}\right\}. \end{array}\right] \quad \textbf{(3)}$$

The networks presented in (3) can be used to formulate the fitness function of model (1) by introducing mean squared error function as follow:

$$\in = \in_1 + \in_2 + \in_3 + \in_4 \quad \textbf{(4)}$$

$$\in_1 = \frac{1}{N}\sum_{m=1}^{N}\left(\frac{dT_m}{dt} - r * T_m\left(1 - \frac{T_m + I_m}{T_{Max}}\right) + \alpha T_m - q + kV_m T_m\right)^2, \quad \textbf{(5)}$$

$$\in_2 = \frac{1}{N}\sum_{m=1}^{N}\left(\frac{dI_m}{dt} + \beta I_m - kV_m T_m\right)^2, \quad \textbf{(6)}$$

$$\in_3 = \frac{1}{N}\sum_{m=1}^{N}\left(\frac{dV_m}{dt} + \gamma V_m - n\beta I_m\right)^2, \quad \textbf{(7)}$$

$$\in_4 = \frac{1}{3}\left(\left(\hat{T}_0 - r_1\right)^2 + \left(\hat{I}_0 - r_2\right)^2 + \left(\hat{V}_0 - r_3\right)^2\right). \quad \textbf{(8)}$$

where $N = 1/h$, $\hat{T}_m$, $\hat{I}_m$, and $\hat{V}_m$ are discrete equivalents of networks for $t_m = mh$, $\in_1$, $\in_2$ and $\in_3$ are the error functions related to respective differential equations of model (1), while $\in_4$ is a part of fitness function representing the initial condition of model (1). The solution of the model (1) can be achieved from with weights such that $\in \to 0$, then, the approximate solutions $\left[\hat{T}, \hat{I}, \hat{V}\right]$ become identical, *i.e.*, $\left[\hat{T}, \hat{I}, \hat{V}\right] \to [T, I, V]$.

2.2. Optimization process: GA-SQP

The optimization of ANNs weights is achieved through the hybrid-computing framework based on GA-SQP in the presented study for solving HIV infection spread model.

Genetic Algorithm is used for constrained/ unconstrained optimization problems based on mathematical modelling of natural genetic cycle in human beings. GA works continually to change the population of individuals, i.e., candidate solutions, and solve numerous problems/tasks of optimization, e.g. stochastic, highly nonlinear and non-differentiable. GA is applied in a variety of fields as a proficient global search tool that works with its reproduction implements via selection, crossover and mutation operators for finding the feasible solution. The schematic work flow of GA in terms of process block structure is presented in Fig. 1, while descriptive operation of each component of reproduction mechanism for the GAs is given in Fig. 2. The recent use of GAs in broad domain include optimization of nanofluid flow systems [29], building envelope calibration [30], for solving multi depot vehicle routing problem [31], Hammerstein controlled autoregressive models [32], thermal comfort in building design [33], prediction of biosorption capacity [34], missing traffic volume data estimation [35], heterogeneous bin packing [36], heterogeneous computing systems [37], radiobiology applications [38], handling offset in chemical processes [39], nonlinear electric circuit models [40], nonlinear Van der Pol equation based heartbeat dynamics [41], reliability–redundancy allocation problem [42] and multi-stage transmission planning [43].

Active-set Method: ASM is a competent local search technique, which broadly implemented for both constrained/unconstrained convex optimization tasks. The process block structure of ASM is presented in Fig. 1. Recently, ASM is used for optimizations problems include optimization in water distribution system [44], nonlinear control for the turbofan engines [45], contact problems for multi-rigid-body dynamics. [46], large-scale nonsmooth optimization tasks [47] and embedded model predictive control [48].

In the presented study, integrated strength of global search efficacy of GAs and rapid local search competency of ASM, i.e., GA-ASM, is exploited to optimize the decision variables of the networks for finding the solution of system of differential equation representing HIV infection model (1). The pseudocode of hybrid heuristic scheme GA-ASM to train ANN is provided in Table 1 for better understanding and ease in reproduction of the results. The necessary parameter settings for both GA and ASMs is also tabulated in Table 1 and the performance of GA-ASM is dependent of these settings. A slight alternation in the said parameters can lead to premature convergence of the optimization process, thus, a lot of simulations, experience and knowledge of underlying optimization concepts is required for realization of appropriate settings for hybrid GA-ASM.

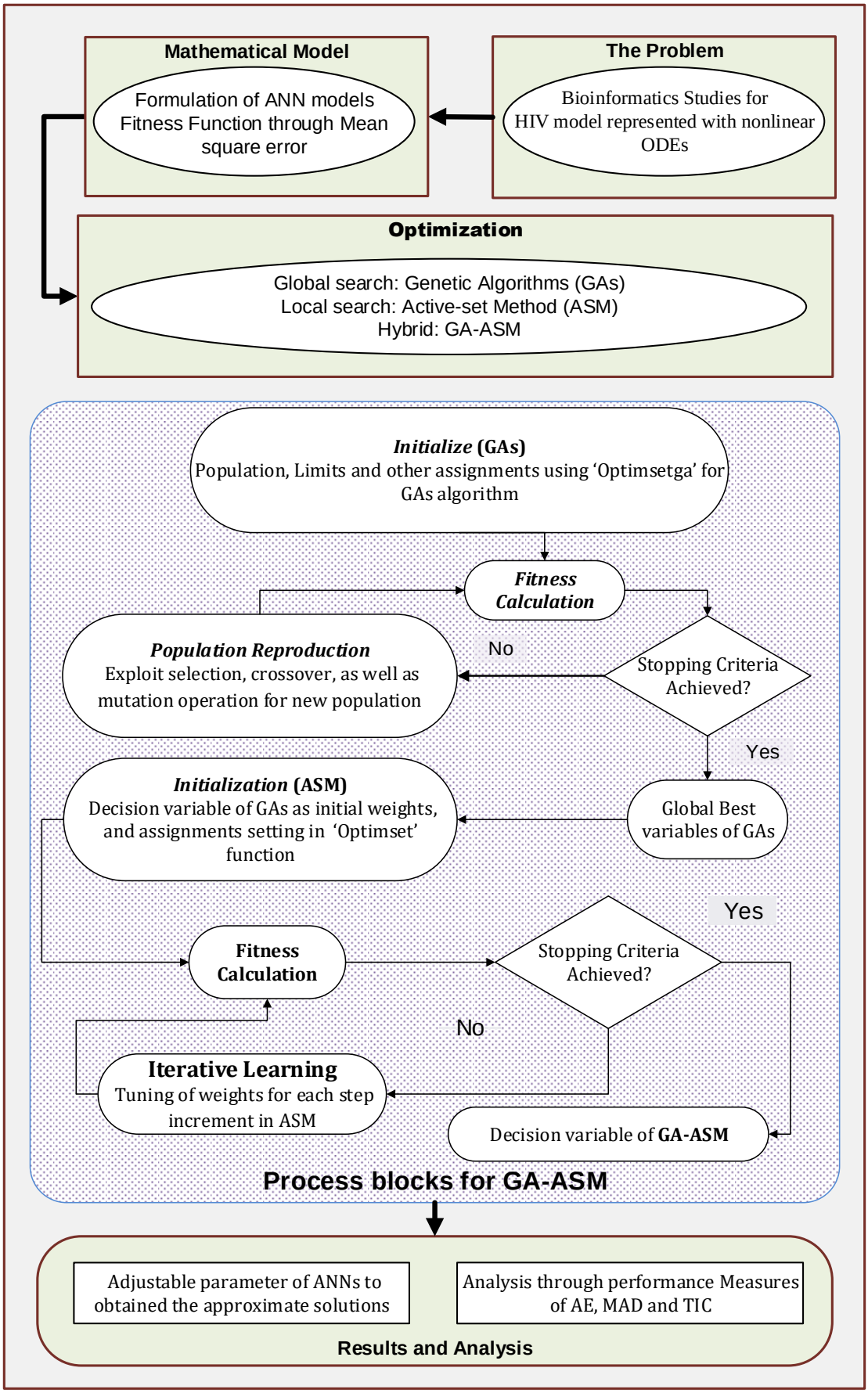

Figure 1: Graphical illustration of present scheme for HIV model

Table 1: Pseudo code using GA-SQP

Start of Genetic Algorithms

Inputs: The chromosome with same number of entries of the network

$$\boldsymbol{W} = [\boldsymbol{W}_T, \boldsymbol{W}_I, \boldsymbol{W}_V] = [(\boldsymbol{\varphi}_T, \boldsymbol{w}_T, \boldsymbol{b}_T), (\boldsymbol{\varphi}_I, \boldsymbol{w}_I, \boldsymbol{b}_I), (\boldsymbol{\varphi}_V, \boldsymbol{w}_V, \boldsymbol{b}_V)]$$

Population: The set of chromosomes to form a population P as:

$$\boldsymbol{P} = [(\boldsymbol{W}_1, \boldsymbol{W}_2, \boldsymbol{W}_3, ..., \boldsymbol{W}_n)], \text{ or}$$

$$\boldsymbol{P} = [(\boldsymbol{W}_{T1}, \boldsymbol{W}_{I1}, \boldsymbol{W}_{V1}, \boldsymbol{W}_{T2}, \boldsymbol{W}_{I2}, \boldsymbol{W}_{V2}, ..., \boldsymbol{W}_{Tn}, \boldsymbol{W}_{In}, \boldsymbol{W}_{Vn})]$$

for $[\boldsymbol{W}_{Ti}, \boldsymbol{W}_{Ii}, \boldsymbol{W}_{Vi}] = [(\boldsymbol{\varphi}_{Ti}, \boldsymbol{w}_{Ti}, \boldsymbol{b}_{Ti}), (\boldsymbol{\varphi}_{Ii}, \boldsymbol{w}_{Ii}, \boldsymbol{b}_{Ii}), (\boldsymbol{\varphi}_{Vi}, \boldsymbol{w}_{Vi}, \boldsymbol{b}_{Vi})]$

Output: Global best variables attained by GAs, $\boldsymbol{W}_{B\_GA}$.

Initialization: Produce $\boldsymbol{W}$ of real numbers to represent a chromosome to make an initial $\boldsymbol{P}$. Set the procedure of Generation and declarations values of "GA" and "gaoptimset" procedures

Calculations of Fitness: To calculate the fitness $\in$ use Eq. (4)

Termination: Implementation of the scheme terminates for accomplishment of the following

'Fitness limit'→ 'e ≤ 10^{-12}, 'Generations'='100', 'TolFun'≤10^{-18}, 'TolCon'≤10^{-20}, 'StallGenLimit'='100','PopulationSize'='300' and other values as 'default' settings.

Go to **storage** step, If termination condition meets,

Ranking: Each $\boldsymbol{W}$ of $\boldsymbol{P}$ ranked through brilliance of the fitness rate.

Reproduction: Repeated the updated $\boldsymbol{P}$ with following

- "Selection": '@selectionuniform'.
- "Crossover": '@crossoverheuristic routine'.
- "Mutations": '@mutationadaptfeasible function'.
- "Elitism": 'best chromosome of $\boldsymbol{P}$'.

Continue from **fitness** step

Storage: Store $\boldsymbol{W}_{B\_GA}$, fitness, generation, time, and count of functions for the present run of GAs

End Genetic algorithms

ASM Procedure Start

Inputs: $\boldsymbol{W}_{B\_GA}$

Output: The best vector of decision variable by GA-ASM is $\boldsymbol{W}_{GA\_ASM}$

Initialize: Use $\boldsymbol{W}_{B\_GA}$ as a starting point, Decelerations and bounded based on "optimset" and "fmincon" routines,

Termination: When any of the value meet, stop the algorithm

'Fitness limit' = '∈ ≤ 10^{-14}', 'total Iterations' = '1200', 'TolFun' ≤ '10^{-18}', 'TolX' ≤ '10^{-22}', 'TolCon' ≤ '10^{-22}', 'MaxFunEvals' ≤ '270000'

While (Terminate)

Fitness calculation: Using Eqs (4-8), find the fitness ∈

Adjustments: Invoking 'fmincon' routine using algorithm 'active-set' to adjust $\boldsymbol{W}$.

Go to the fitness step with updated $\boldsymbol{W}$

End

Save the final adaptive weights $\boldsymbol{W}_{GA\_SQP}$ *and* ∈,iterations, time and function count for the current run.

ASM Procedure End

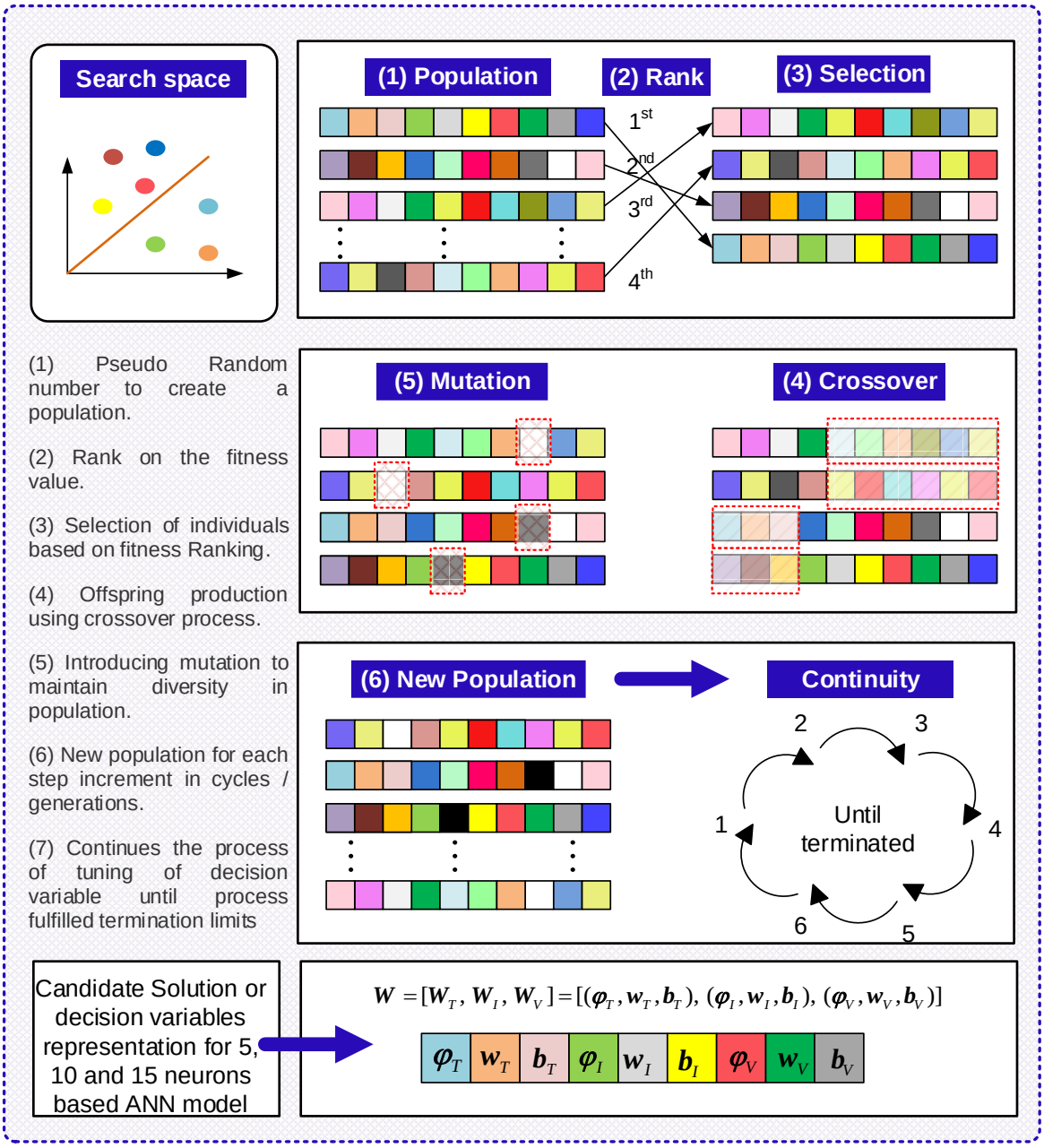

Figure 2: Optimization cycle of Genetic Algorithms

3. Performance indices

The two performance measures for the model (1) are introduced here based on the mean absolute deviation (MAD) and Theil's inequality coefficient (TIC). The mathematical formulation of both MAD and TIC metrics is given, respectively, as follows:

$$\left[MAD_T, MAD_I, MAD_V\right] = \left[\frac{1}{m}\sum_{i=1}^{m}\left|T_i - \hat{T}_i\right|, \frac{1}{m}\sum_{i=1}^{m}\left|I_i - \hat{I}_i\right|, \frac{1}{m}\sum_{i=1}^{m}\left|V_i - \hat{V}_i\right|\right], \quad \textbf{(9)}$$

$$[\mathrm{TIC}_T,\mathrm{TIC}_I,\mathrm{TIC}_V]=\left(\frac{\sqrt{\frac{1}{m}\sum_{i=1}^{m}\left(T_i-\hat{T}_i\right)^2}}{\left(\sqrt{\frac{1}{m}\sum_{i=1}^{m}T_i^2}+\sqrt{\frac{1}{m}\sum_{i=1}^{m}\hat{T}_i^2}\right)},\frac{\sqrt{\frac{1}{m}\sum_{i=1}^{m}\left(I_i-\hat{I}_i\right)^2}}{\left(\sqrt{\frac{1}{m}\sum_{i=1}^{m}I_i^2}+\sqrt{\frac{1}{m}\sum_{i=1}^{m}\hat{I}_i^2}\right)},\frac{\sqrt{\frac{1}{m}\sum_{i=1}^{m}\left(V_i-\hat{V}_i\right)^2}}{\left(\sqrt{\frac{1}{m}\sum_{i=1}^{m}V_i^2}+\sqrt{\frac{1}{m}\sum_{i=1}^{m}\hat{V}_i^2}\right)}\right)., \qquad \textbf{(10)}$$

The terms arising in equations (9-10) are defined in the last section.

3. Results and discussion

In this section, the HIV infection model (1) is solved numerically by taking different number of neurons based layered structure neural network optimized with integrated heuristics of GA-ASM as per process narrated in pseudocode tabulated in Table 1. The comparison of presented results and the RK solution is used to analyze the exactness of the proposed solver. Moreover, results of statistical analysis are also used to check the accuracy of the present scheme.

HIV infection model of CD4+ T cells as given in equation (1) with reported parametric values $r = 3$, $q = 0.1$, $\alpha = 0.02$, $\gamma = 2.4$, $\beta = 0.3$, $n = 10$, $k = 0.0027$, $T_{max} = 1500$ and $r_1 = r_2 = r_3 = 0$, are taken for numerical experimentation of presented methodology [49-53]. The updated form of the model (1) with these parameters is written as follows:

$$\begin{cases} \dfrac{dT}{dt} = 3T\left(1-\dfrac{T+I}{1500}\right)-0.02T+0.1-0.0027VT, & T(0)=0.1 \\ \dfrac{dI}{dt} = -0.3I+0.0027VT, & I(0)=0 \\ \dfrac{dV}{dt} = -2.4V+3I, & V(0)=0.1 \end{cases} \qquad \textbf{(11)}$$

The error based objective function for model (11) is written as:

$$\in=\frac{1}{N}\sum_{m=1}^{N}\left(\begin{array}{l}\left[\dfrac{dT_m}{dt}-3T_m\left(1-\dfrac{T_m+I_m}{1500}\right)+0.02T_m-0.1+0.0027V_mT_m\right]^2 \\ +\left[\dfrac{dI_m}{dt}+0.3I_m-0.0027V_mT_m\right]^2+\left[\dfrac{dV_m}{dt}+2.4V_m-3I_m\right]^2\end{array}\right) \qquad \textbf{(12)}$$
$$+\frac{1}{3}\left(\left(\hat{T}_0-0.1\right)^2+\left(\hat{I}_0\right)^2+\left(\hat{V}_0-0.1\right)^2\right),$$

The terms arising in relation (12) are defined in section 2. The optimization of the relation (12) is carried out with GA-ASM for hundred trials and one set of trained weight of ANN based on 5, 10 and 15 neuron is plotted in Fig. 3 for $\hat{T}$, $\hat{I}$, and $\hat{V}$. The parameters presented in Fig. 3 are used to find the approximate solution for $\hat{T}$, $\hat{I}$, and $\hat{V}$ using equation (1) of set (3). The solutions determined for ANN models of equation with 5, 10 and 15 neurons in case of

$\hat{T}$ and $\hat{V}$ along with reference solutions of RK solver are presented in Fig. 4. The overlapping outcomes of presented method with RK solver for all three neuron based ANN models is obtained. In order to estimate matching accuracy, the absolute error (AE) is calculated and results are also plotted in Fig. 4 for 5, 10 and 15 neuron based models for all three $\hat{T}$, $\hat{I}$, and $\hat{V}$ parameters. It is clear that the values of $\hat{T}$, $\hat{I}$, and $\hat{V}$ lie in the ranges of 10^{-05} to 10^{-07}, respectively, for 5 neuron models of HIV infection system, while for 10 and 15 neuron based models lie around 10^{-05} to 10^{-07} and 10^{-06} to 10^{-08}, respectively. The present results are found in good agreement with the RK solver for HIV infection model of $CD4^{+}$ cells.

Result of statistics of proposed methodology for 100 independent trials are presented in Figures 5, 6 and 7 for both performance indices of MAD and TIC in case of 5, 10 and 15 number of neurons based ANN models, respectively. In subfigures 5(a), 6(a) and 7(a) MAD based values of $\hat{T}$, $\hat{I}$, and $\hat{V}$ for number of trials are present, while in case of TIC results are illustrated in subfigures 5(n), 6(n) and 7(n). Assessment of the precision of proposed stochastic solver is performed by histogram studies and boxplots for all three neuron based model. The results of histogram are provided in subfigures 5(b-d, h-j), 6(b-d, h-j) and 7(b-d, h-j), while boxplots are given in 5(e-g, k-m), 6(e-g, k-m) and 7(e-g, k-m). Results of histogram/boxplots studies show that around 80% of independent executions/trials of presented scheme achieve accuracy of order 10^{-06} and 10^{-08} for MAD and TIC, respectively. With increase in number of neurons, i.e., in case of 5, 10 and 15, the accuracy also enhanced accordingly for ANN based differential equation models of HIV infection system (11). A small values of median in each boxplot show the consistent precision of proposed stochastic solver for HIV infection model (11).

Statistical measures based on minimum (Min), median (Med) and semi interquartile range (SIR) are conducted for precision analysis of the present stochastic technique. The statistics for Min, Med and SIR terms are tabulated in Tables 3, 4 and 5 for 5, 10 and 15 number of neurons based ANN models, respectively. For $T(t)$, Min values lies around 10^{-06} to 10^{-09} for all neurons based models of ANN, while the Med values lie around 10^{-03} to 10^{-05} for 5 neurons, whereas for both 10 and15 neurons the values lie around 10^{-04} to 10^{-06}. Finally, the SIR values of $T(t)$ are also provided for each case of HIV model. SIR is basically one half of the difference of 3rd quartile (Q_3=75% data) and 1st quartile (Q_1= 25% data). The values of the SIR lie around 10^{-04} to 10^{-06} that indicates very good ranges for HIV model. Moreover, $I(t)$ and $V(t)$ similar trend of the results is observed.

Table 2: Statistics results for metrics for 5 neurons based ANN model of HIV model

x	$T(t)$			$I(t)$			$V(t)$		
	Min	**Med**	**SIR**	**Min**	**Med**	**SIR**	**Min**	**Med**	**SIR**
0	6.21E-08	2.59E-05	1.61E-02	1.68E-05	9.03E-05	1.48E-05	6.63E-09	1.46E-06	2.09E-06
0.2	5.31E-08	1.08E-04	4.62E-02	2.18E-05	1.15E-04	1.54E-05	5.62E-06	5.95E-05	1.63E-05
0.4	4.24E-07	2.57E-04	8.54E-02	2.42E-05	1.35E-04	1.53E-05	2.92E-05	1.04E-04	3.04E-05
0.6	1.38E-06	3.18E-04	1.56E-01	1.75E-05	1.50E-04	1.74E-05	1.71E-05	1.29E-04	2.90E-05
0.8	3.25E-09	6.98E-04	2.81E-01	5.77E-05	1.67E-04	1.97E-05	2.83E-05	1.60E-04	2.88E-05
1	1.81E-06	1.17E-03	5.07E-01	1.06E-04	1.84E-04	2.06E-05	3.34E-05	1.77E-04	2.59E-05

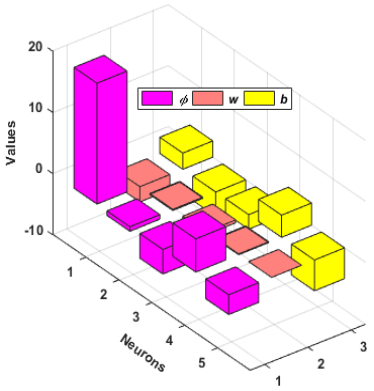

(a): ANN weights of 5 neurons for $T(t)$ of HIV infection model

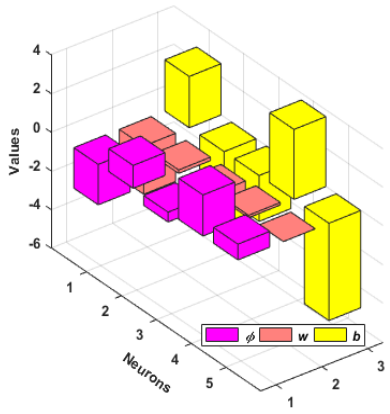

(b): ANN weights of 5 neurons for $I(t)$ of HIV infection model

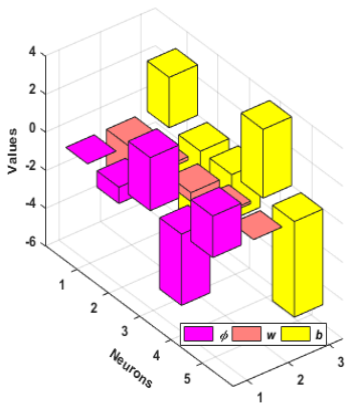

(c): ANN weights of 5 neurons for $V(t)$ of HIV infection model

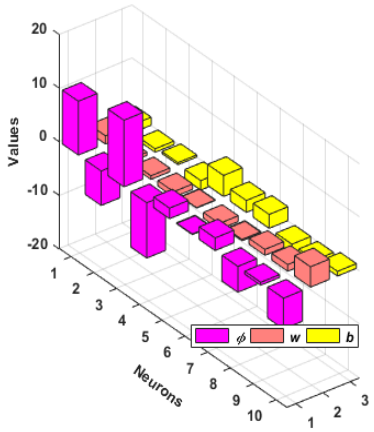

(d): ANN weights of 10 neurons for $T(t)$ of HIV infection model

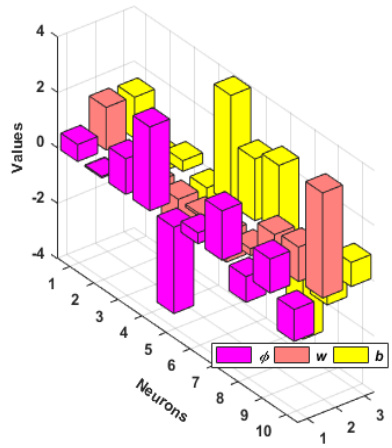

(e): ANN weights of 10 neurons for $I(t)$ of HIV infection model

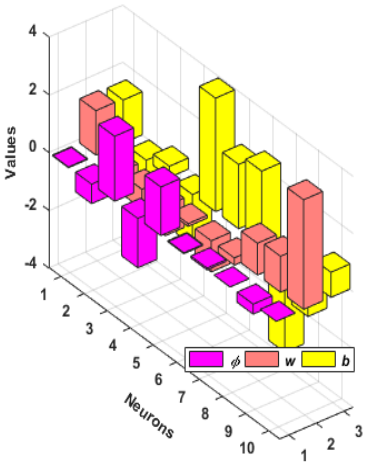

(f): ANN weights of 10 neurons for $V(t)$ of HIV infection model

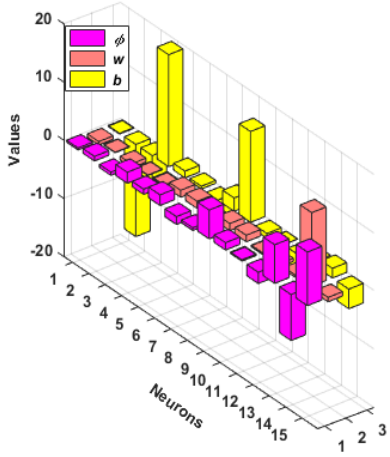

(g): ANN weights of 15 neurons for $T(t)$ of HIV infection model

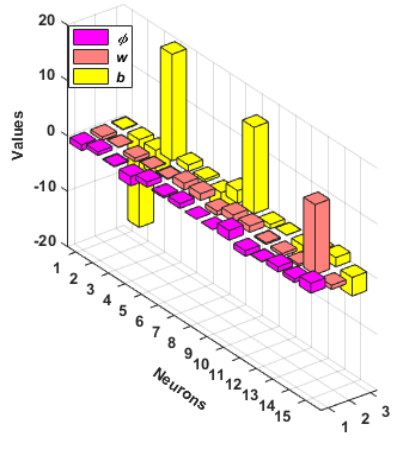

(h): ANN weights of 15 neurons for $I(t)$ of HIV infection model

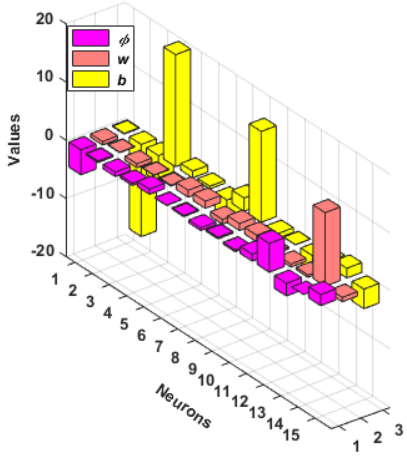

(i): ANN weights of 15 neurons for $V(t)$ of HIV infection model

Figure 3: A set of weights of ANNs trained by GA-ASM using for 5, 10 and 15 neurons based differential equations models of HIV infection system of CD4+ T cells

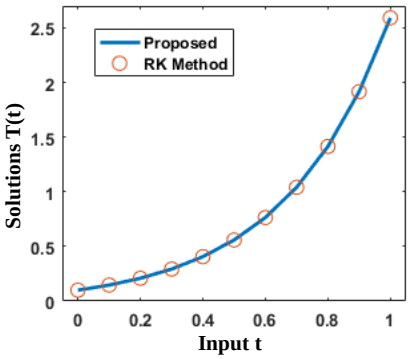

(a): Comparison of the solution $T(t)$ of HIV infection mode for 5 neurons

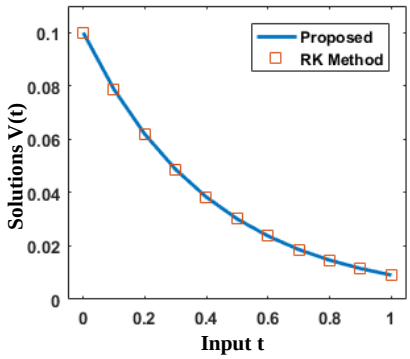

(a): Comparison of the solution $TV(t)$ of HIV infection mode for 5 neurons

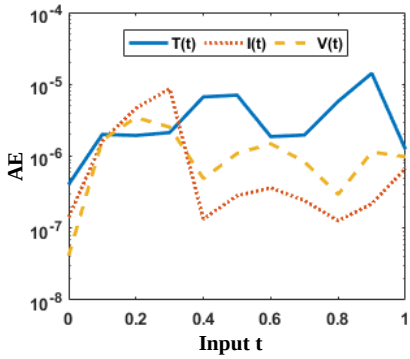

(c): Comparison on AE for HIV infection model for 5 neurons

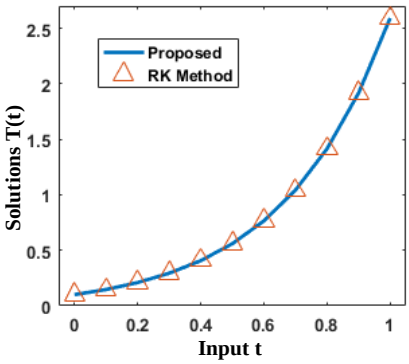

(d): Comparison of the solution $T(t)$ of HIV infection mode for 10 neurons

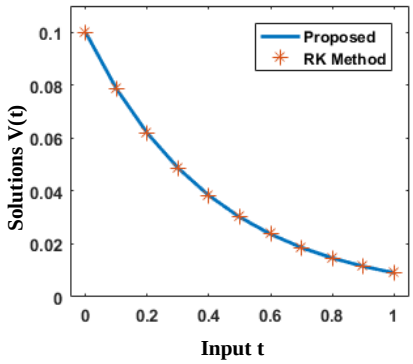

(e): Comparison of the solution $TV(t)$ of HIV infection mode for 10 neurons

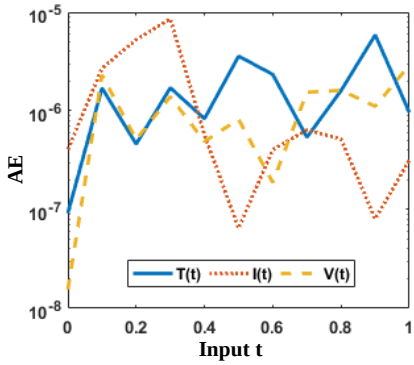

(f): Comparison on AE for HIV infection model for 10 neurons

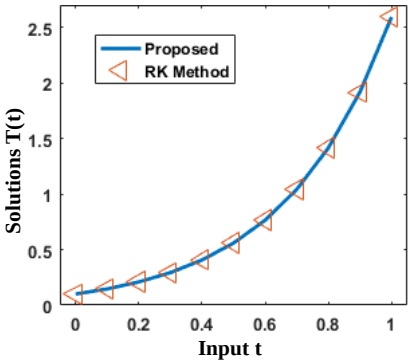

(g): Comparison of the solution $T(t)$ of HIV infection mode for 15 neurons

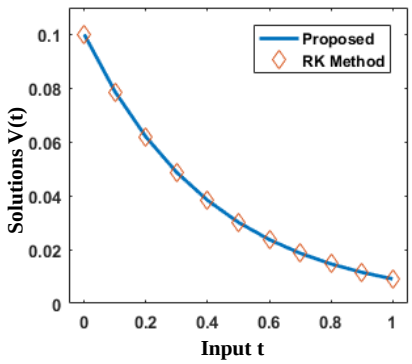

(h): Comparison of the solution $V(t)$ of HIV infection mode for 15 neurons

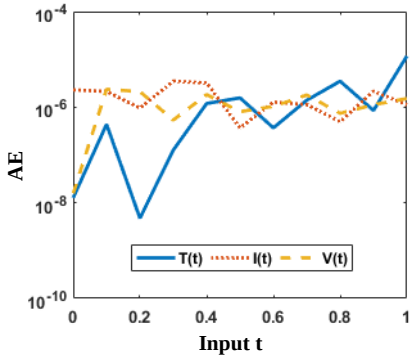

(i): Comparison on AE for HIV infection model for 15 neurons

Figure 4: Results of proposed methodology and their comparison from reference RK solver for 5, 10 and 15 neurons based ANN models of differential equation.

Table 3: Statistics results for metrics for 10 neurons based ANN model of HIV model

x	$T(t)$			$I(t)$			$V(t)$		
	Min	**Med**	**SIR**	**Min**	**Med**	**SIR**	**Min**	**Med**	**SIR**
0	1.93E-08	1.12E-06	1.23E-06	5.19E-05	8.98E-05	3.38E-07	5.66E-09	2.48E-07	3.10E-07
0.2	3.68E-07	2.44E-05	1.48E-05	1.41E-06	1.10E-04	4.14E-06	2.68E-05	5.51E-05	6.75E-06
0.4	7.64E-08	2.89E-05	1.73E-05	1.11E-05	1.26E-04	6.18E-06	8.83E-06	8.67E-05	5.59E-06
0.6	4.18E-07	6.14E-05	3.57E-05	3.51E-05	1.42E-04	5.41E-06	2.97E-05	1.17E-04	5.64E-06
0.8	2.42E-06	1.06E-04	6.12E-05	8.14E-05	1.58E-04	2.13E-06	3.25E-05	1.47E-04	4.39E-06
1	3.97E-07	1.69E-04	1.07E-04	9.98E-05	1.76E-04	3.17E-06	6.72E-05	1.71E-04	6.68E-06

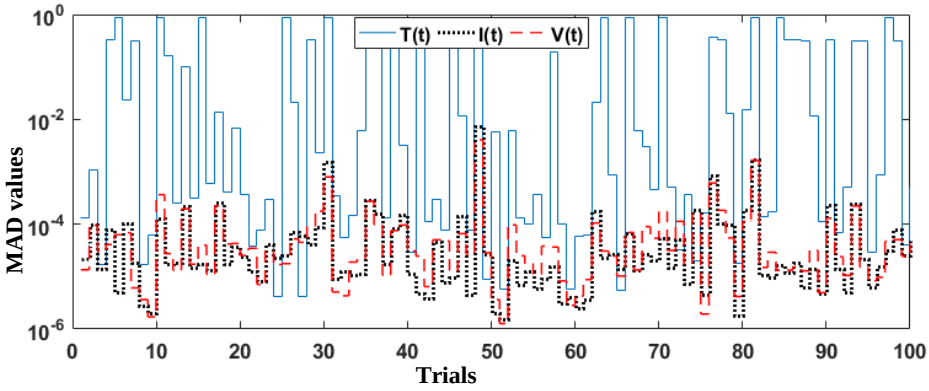

(a) Analysis on MAD values

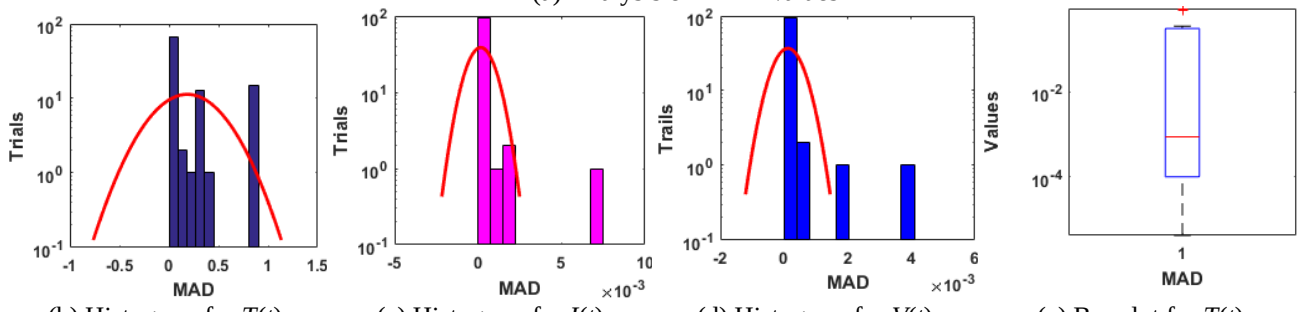

(b) Histogram for $T(t)$ (c) Histogram for $I(t)$ (d) Histogram for $V(t)$ (e) Boxplot for $T(t)$

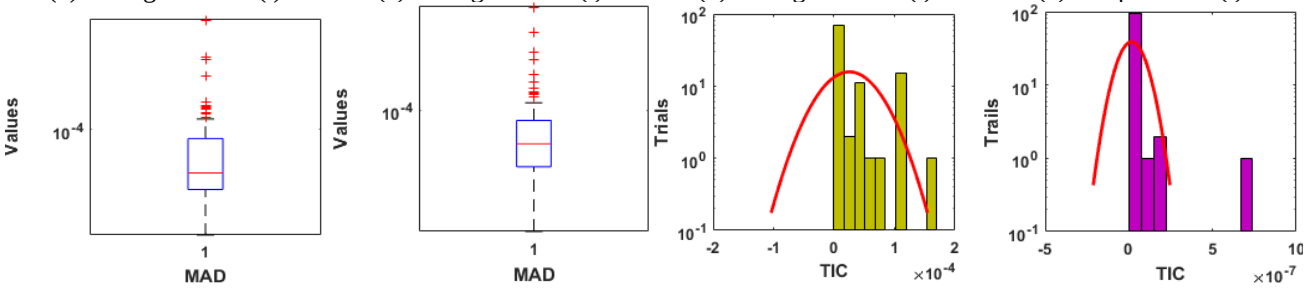

(f) Boxplot for $I(t)$ (g) Boxplot for $V(t)$ (h) Histogram for $T(t)$ (i) Histogram for $I(t)$

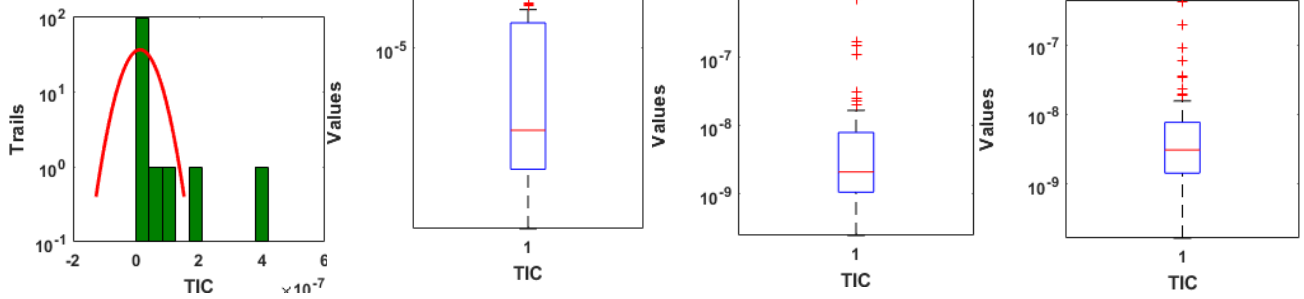

(j) Histogram for $V(t)$ (k) Boxplot for $T(t)$ (l) Boxplot for $I(t)$ (m) Boxplot for $V(t)$

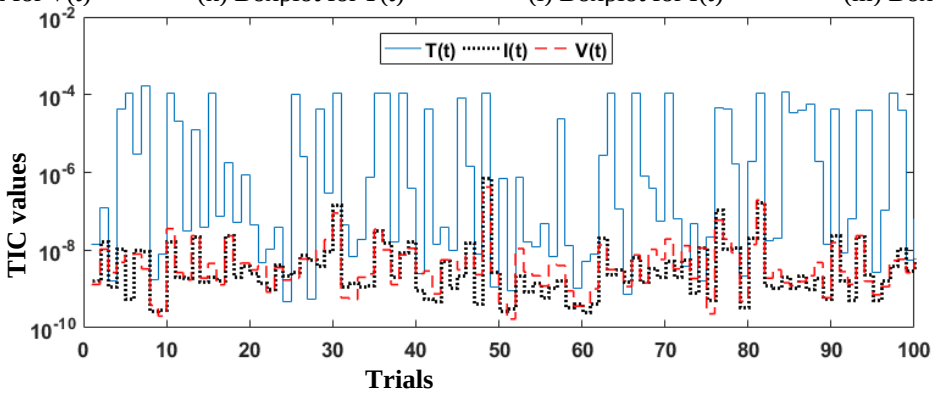

(n) Analysis on TIC values

Figure 5: Statistics for MAD and TIC values with the histograms and boxplot for 5 neurons

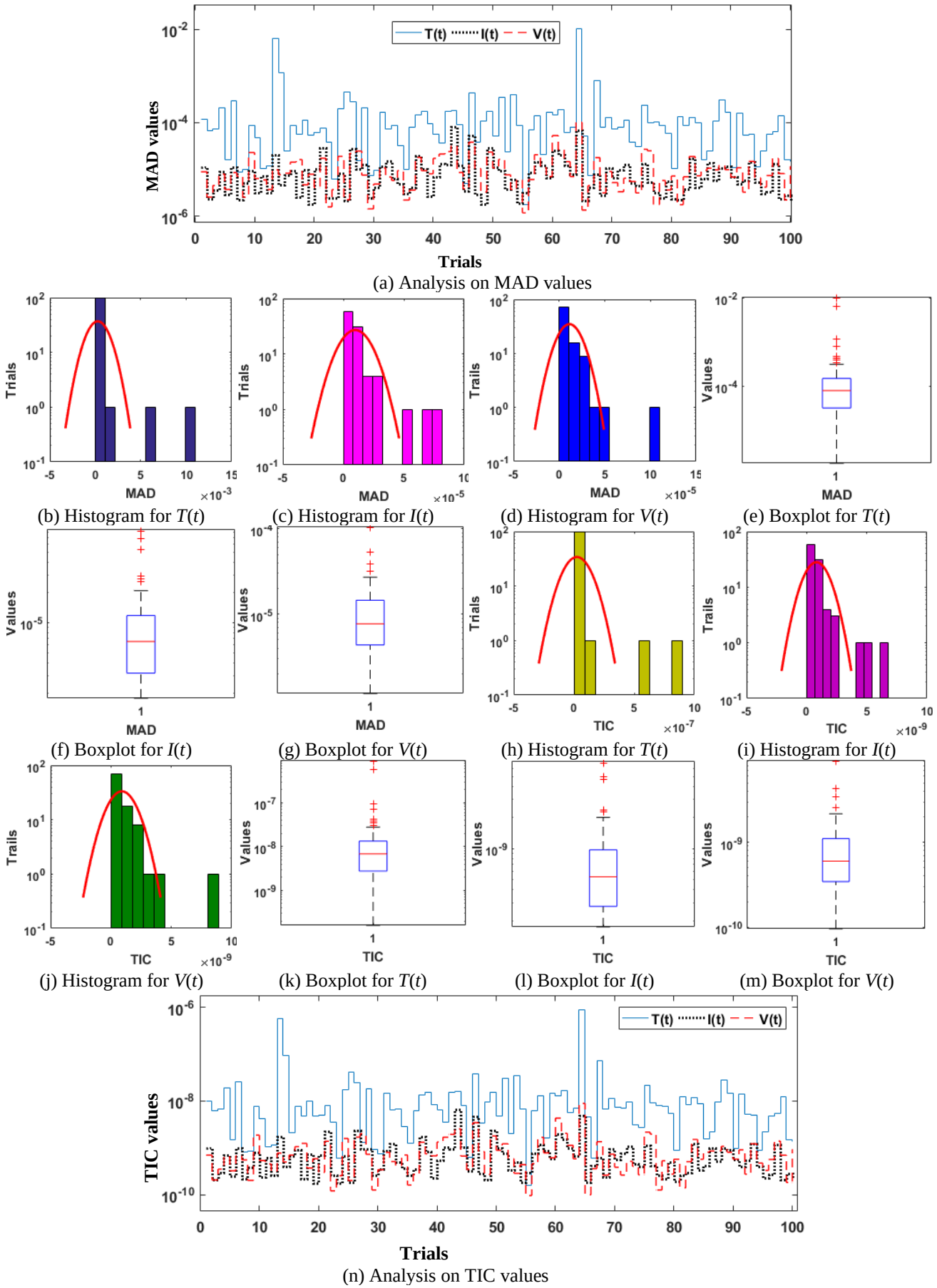

(a) Analysis on MAD values

(b) Histogram for $T(t)$ (c) Histogram for $I(t)$ (d) Histogram for $V(t)$ (e) Boxplot for $T(t)$

(f) Boxplot for $I(t)$ (g) Boxplot for $V(t)$ (h) Histogram for $T(t)$ (i) Histogram for $I(t)$

(j) Histogram for $V(t)$ (k) Boxplot for $T(t)$ (l) Boxplot for $I(t)$ (m) Boxplot for $V(t)$

(n) Analysis on TIC values

Figure 6: Statistics for MAD and TIC values with the histograms and boxplot for 10 neurons

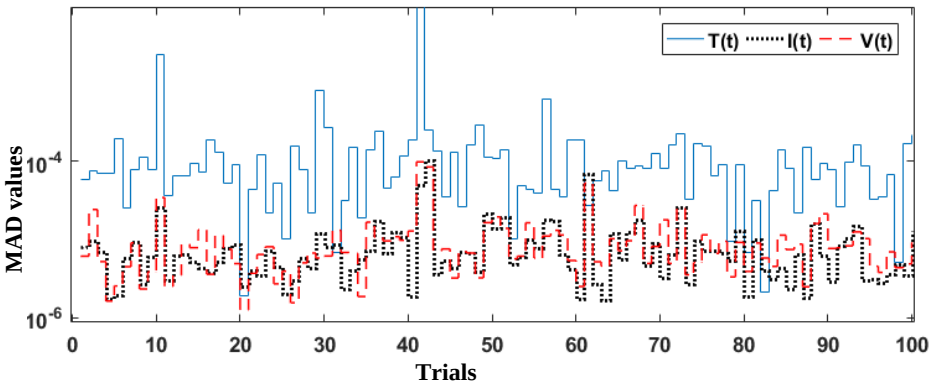

(a) Analysis on MAD values

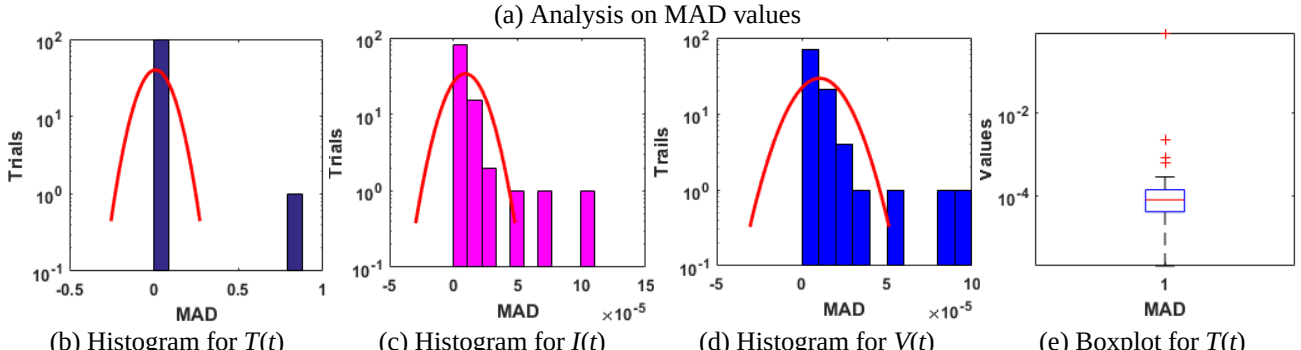

(b) Histogram for $T(t)$ (c) Histogram for $I(t)$ (d) Histogram for $V(t)$ (e) Boxplot for $T(t)$

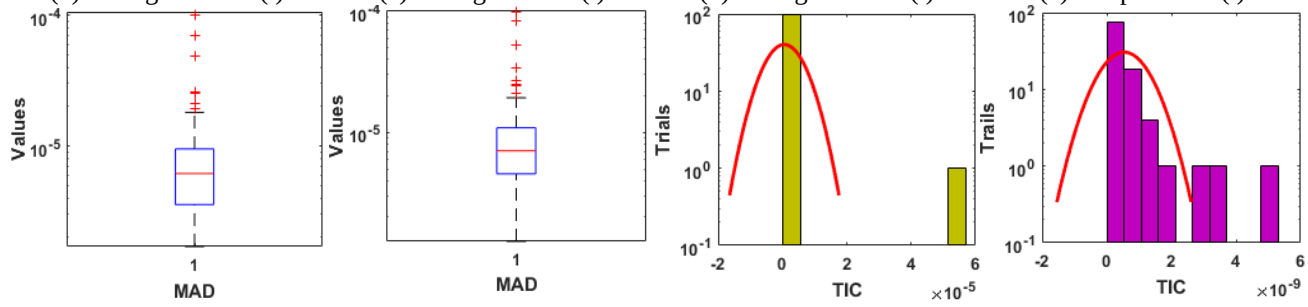

(f) Boxplot for $I(t)$ (g) Boxplot for $V(t)$ (h) Histogram for $T(t)$ (i) Histogram for $I(t)$

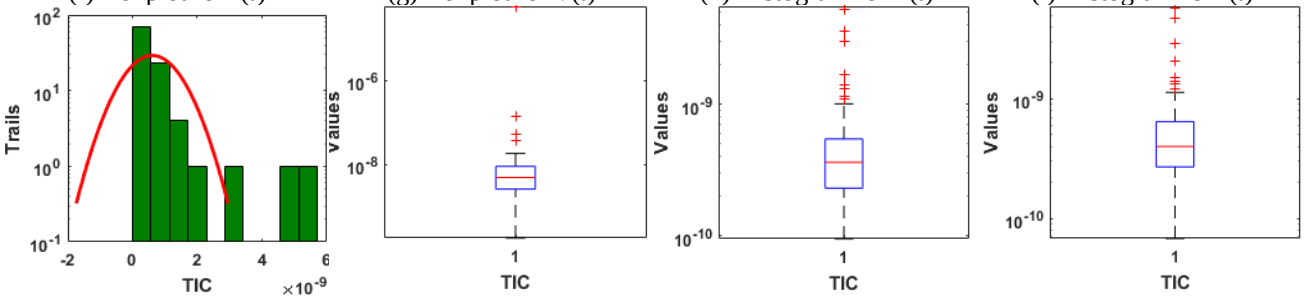

(j) Histogram for $V(t)$ (k) Boxplot for $T(t)$ (l) Boxplot for $I(t)$ (m) Boxplot for $V(t)$

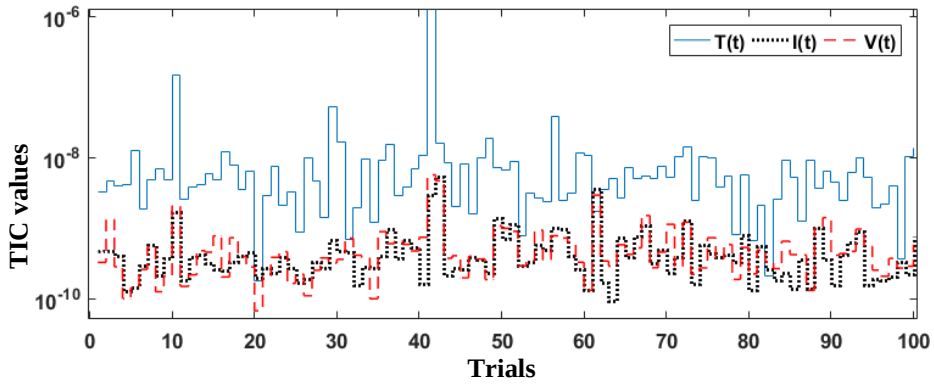

(n) Analysis on TIC values

Figure 7: Statistics for MAD and TIC values with the histograms and boxplot for 15 neurons

Table 4: Statistics results for metrics for 15 neurons based ANN model of HIV model

x	$T(t)$			$I(t)$			$V(t)$		
	Min	**Med**	**SIR**	**Min**	**Med**	**SIR**	**Min**	**Med**	**SIR**
0	1.57E-08	1.04E-06	9.78E-07	6.74E-05	8.98E-05	3.64E-07	7.74E-10	2.49E-07	2.96E-07
0.2	1.24E-06	2.82E-05	1.66E-05	7.76E-05	1.10E-04	3.87E-06	2.93E-05	5.52E-05	8.34E-06
0.4	3.67E-07	3.08E-05	2.03E-05	7.44E-05	1.27E-04	5.81E-06	6.50E-05	8.49E-05	5.33E-06
0.6	1.16E-06	7.30E-05	4.54E-05	9.26E-05	1.43E-04	3.21E-06	4.88E-05	1.20E-04	5.97E-06
0.8	2.98E-06	1.23E-04	8.31E-05	1.41E-04	1.58E-04	1.97E-06	9.93E-05	1.48E-04	5.20E-06
1	1.89E-07	2.10E-04	1.37E-04	1.41E-04	1.76E-04	3.12E-06	1.48E-04	1.67E-04	5.51E-06

4. Conclusions

A novel stochastic computing paradigm is designed to solve nonlinear HIV model of bioinformatics using different neurons based models of neural networks optimized with integrated heuristics of global capability of genetic algorithms and rapid fine tuning of decision variables by exploitation of local search strength of active-set method. The HIV model is effectively evaluated by proposed computing paradigm with layer structure based neural networks models for 5, 10 and 15 neurons and accuracy of numerical results enhanced by larger neurons based networks. The accuracy of the stochastic scheme is established by obtaining the overlapping results with Runge-Kutta numerical scheme having 4 to 6 decimal places of matching for solving HIV model. Statistical observations, based on 100 executions/trials to solve HIV model, in terms of magnitudes of mean, median, semi interquartile range and standard deviation metrics validate the accurateness, trustworthiness and robustness of the algorithm which is further endorsed by performance indices of MAD and TIC.

In future, the presented scheme is a promising alternative solver to be explored/exploited for the solution of stiff and non-stiff nonlinear systems arising in the fields of fluid dynamics, astrophysics, nanotechnology, atomic physics, electric circuit theory, plasma physics and bioinformatics.

References

[1] Perelson, A.S., Kirschner, D.E. and De Boer, R., 1993. Dynamics of HIV infection of CD4+ T cells. Mathematical biosciences, 114(1), pp.81-125.

[2] Ongun, M.Y., 2011. The Laplace adomian decomposition method for solving a model for HIV infection of CD4+ T cells. Mathematical and Computer Modelling, 53(5-6), pp.597-603.

[3] Merdan, M., 2007. Homotopy perturbation method for solving a model for HIV infection of CD4+ T cells.

[4] Dogan, N., 2012. Numerical treatment of the model for HIV infection of CD4+ T cells by using multistep Laplace Adomian decomposition method. Discrete Dynamics in Nature and Society, 2012.

[5] Merdan, M., Gökdoğan, A. and Yildirim, A., 2011. On the numerical solution of the model for HIV infection of CD4+ T cells. Computers & Mathematics with Applications, 62(1), pp.118-123.

[6] Yüzbaşı, Ş., 2012. A numerical approach to solve the model for HIV infection of CD4+ T cells. Applied Mathematical Modelling, 36(12), pp.5876-5890.

[7] Srivastava, V.K., Awasthi, M.K. and Kumar, S., 2014. Numerical approximation for HIV infection of CD4+ T cells mathematical model. Ain Shams Engineering Journal, 5(2), pp.625-629.

[8] Raja, M.A.Z., Shah, Z., Manzar, M.A., Ahmad, I., Awais, M. and Baleanu, D., 2018. A new stochastic computing paradigm for nonlinear Painlevé II systems in applications of random matrix theory. *The European Physical Journal Plus*, *133*(7), p.254.

[9] Munir, A., et al., 2019. Intelligent computing approach to analyze the dynamics of wire coating with Oldroyd 8-constant fluid. *Neural Computing and Applications*, *31*(3), pp.751-775.

[10] Yadav, N., Yadav, A., Kumar, M. and Kim, J.H., 2017. An efficient algorithm based on artificial neural networks and particle swarm optimization for solution of nonlinear Troesch's problem. Neural Computing and Applications, 28(1), pp.171-178.

[11] Hassan, A., Kamran, M., Illahi, A. and Zahoor, R.M.A., 2019. Design of cascade artificial neural networks optimized with the memetic computing paradigm for solving the nonlinear Bratu system. *The European Physical Journal Plus*, *134*(3), p.122.

[12] Mehmood, A., Zameer, A. and Raja, M.A.Z., 2018. Intelligent computing to analyze the dynamics of magnetohydrodynamic flow over stretchable rotating disk model. *Applied Soft Computing*, *67*, pp.8-28.

[13] Raja, M.A.Z., Shah, F.H., Tariq, M. and Ahmad, I., 2018. Design of artificial neural network models optimized with sequential quadratic programming to study the dynamics of nonlinear Troesch's problem arising in plasma physics. Neural Computing and Applications, 29(6), pp.83-109.

[14] Momani, S., Abo-Hammour, Z.S. and Alsmadi, O.M., 2016. Solution of inverse kinematics problem using genetic algorithms. Applied Mathematics & Information Sciences, 10(1), p.225.

[15] Schaff, J.C., Gao, F., Li, Y., Novak, I.L. and Slepchenko, B.M., 2016. Numerical approach to spatial deterministic-stochastic models arising in cell biology. PLoS computational biology, 12(12), p.e1005236.

[16] Umar, M., Sabir, Z. and Raja, M.A.Z., 2019. Intelligent computing for numerical treatment of nonlinear prey–predator models. Applied Soft Computing, 80, pp.506-524.

[17] Pelletier, F., Masson, C. and Tahan, A., 2016. Wind turbine power curve modelling using artificial neural network. Renewable Energy, 89, pp.207-214.

[18] Raja, M.A.Z., Khan, J.A. and Haroon, T., 2015. Stochastic numerical treatment for thin film flow of third grade fluid using unsupervised neural networks. Journal of the Taiwan Institute of Chemical Engineers, 48, pp.26-39.

[19] Effati, S. and Pakdaman, M., 2010. Artificial neural network approach for solving fuzzy differential equations. Information Sciences, 180(8), pp.1434-1457.

[20] Soize, C., 2012. Stochastic models of uncertainties in computational structural dynamics and structural acoustics. In Nondeterministic Mechanics (pp. 61-113). Springer, Vienna.

[21] Sabir, Z., Manzar, M.A., Raja, M.A.Z., Sheraz, M. and Wazwaz, A.M., 2018. Neuro-heuristics for nonlinear singular Thomas-Fermi systems. Applied Soft Computing, 65, pp.152-169.

[22] Raja, M.A.Z., Farooq, U., Chaudhary, N.I. and Wazwaz, A.M., 2016. Stochastic numerical solver for nanofluidic problems containing multi-walled carbon nanotubes. Applied Soft Computing, 38, pp.561-586.

[23] Raja, M.A.Z., Umar, M., Sabir, Z., Khan, J.A. and Baleanu, D., 2018. A new stochastic computing paradigm for the dynamics of nonlinear singular heat conduction model of the human head. The European Physical Journal Plus, 133(9), p.364.

[24] Ahmad, I., et al., 2018. Neuro-evolutionary computing paradigm for Painlevé equation-II in nonlinear optics. *The European Physical Journal Plus*, *133*(5), p.184.

[25] Raja, M.A.Z., Mehmood, J., Sabir, Z., Nasab, A.K. and Manzar, M.A., 2019. Numerical solution of doubly singular nonlinear systems using neural networks-based integrated intelligent computing. Neural Computing and Applications, 31(3), pp.793-812.

[26] Mehmood, A., Zameer, A., Raja, M.A.Z., Bibi, R., Chaudhary, N.I. and Aslam, M.S., 2019. Nature-inspired heuristic paradigms for parameter estimation of control autoregressive moving average systems. *Neural Computing and Applications*, *31*(10), pp.5819-5842.

[27] Zhang, Z., El-Moselhy, T.A., Elfadel, I.M. and Daniel, L., 2013. Stochastic testing method for transistor-level uncertainty quantification based on generalized polynomial chaos. IEEE Transactions on Computer-Aided Design of Integrated Circuits and Systems, 32(10), pp.1533-1545.

[28] Zameer, A., at el., 2017. Intelligent and robust prediction of short term wind power using genetic programming based ensemble of neural networks. *Energy conversion and management*, *134*, pp.361-372.

[29] Azad, A.V. and Azad, N.V., 2016. Application of nanofluids for the optimal design of shell and tube heat exchangers using genetic algorithm. Case Studies in Thermal Engineering, 8, pp.198-206.

[30] Ruiz, G.R., Bandera, C.F., Temes, T.G.A. and Gutierrez, A.S.O., 2016. Genetic algorithm for building envelope calibration. Applied energy, 168, pp.691-705.

[31] Karakatič, S. and Podgorelec, V., 2015. A survey of genetic algorithms for solving multi depot vehicle routing problem. Applied Soft Computing, 27, pp.519-532.

[32] Raja, M.A.Z., Shah, A.A., Mehmood, A., Chaudhary, N.I. and Aslam, M.S., 2018. Bio-inspired computational heuristics for parameter estimation of nonlinear Hammerstein controlled autoregressive system. *Neural Computing and Applications*, *29*(12), pp.1455-1474.

[33] Yu, W., Li, B., Jia, H., Zhang, M. and Wang, D., 2015. Application of multi-objective genetic algorithm to optimize energy efficiency and thermal comfort in building design. Energy and Buildings, 88, pp.135-143.

[34] Mishra, P.C. and Giri, A.K., 2017. Prediction of Biosorption Capacity Using Artificial Neural Network Modeling and Genetic Algorithm: Prediction of Biosorption Capacity. In Handbook of Research on Manufacturing Process Modeling and Optimization Strategies (pp. 276-290). IGI Global.

[35] Tang, J., Zhang, G., Wang, Y., Wang, H. and Liu, F., 2015. A hybrid approach to integrate fuzzy C-means based imputation method with genetic algorithm for missing traffic volume data estimation. Transportation Research Part C: Emerging Technologies, 51, pp.29-40.

[36] Sridhar, R., Chandrasekaran, M., Sriramya, C. and Page, T., 2017, March. Optimization of heterogeneous Bin packing using adaptive genetic algorithm. In IOP Conference Series: Materials Science and Engineering (Vol. 183, No. 1, p. 012026). IOP Publishing.

[37] Ahmad, S.G., Liew, C.S., Munir, E.U., Ang, T.F. and Khan, S.U., 2016. A hybrid genetic algorithm for optimization of scheduling workflow applications in heterogeneous computing systems. Journal of Parallel and Distributed Computing, 87, pp.80-90.

[38] Cavallone, M., Flacco, A. and Malka, V., 2019. Shaping of laser-accelerated proton beam for radiobiology applications via genetic algorithm. arXiv preprint arXiv:1903.04787.

[39] Araújo, R.D.B. and Coelho, A.A., 2017. Filtered predictive control design using multi-objective optimization based on genetic algorithm for handling offset in chemical processes. Chemical Engineering Research and Design, 117, pp.265-273.

[40] Mehmood, A., et al., 2019. Integrated computational intelligent paradigm for nonlinear electric circuit models using neural networks, genetic algorithms and sequential quadratic programming. *Neural Computing and Applications*, pp.1-21.

[41] Raja, M.A.Z., Shah, F.H. and Syam, M.I., 2018. Intelligent computing approach to solve the nonlinear Van der Pol system for heartbeat model. Neural Computing and Applications, 30(12), pp.3651-3675.

[42] Kim, H. and Kim, P., 2017. Reliability–redundancy allocation problem considering optimal redundancy strategy using parallel genetic algorithm. Reliability Engineering & System Safety, 159, pp.153-160.

[43] Poubel, R.P.B., De Oliveira, E.J., Manso, L.A.F., Honório, L.M. and Oliveira, L.W., 2017. Tree searching heuristic algorithm for multi-stage transmission planning considering security constraints via genetic algorithm. Electric Power Systems Research, 142, pp.290-297.

[44] Deuerlein, J.W., Piller, O., Elhay, S. and Simpson, A.R., 2018. Content-Based Active-Set Method for the Pressure-Dependent Model of Water Distribution Systems. Journal of Water Resources Planning and Management, 145(1), p.04018082.

[45] Wang, J., Gao, Y., Zhang, W. and Hu, Z., 2019. Nonlinear Control of Turbofan Engines: An Active Set-Based Method for Performance Optimization. Journal of Dynamic Systems, Measurement, and Control, 141(5), p.051014.

[46] Barboteu, M. and Dumont, S., 2018. A primal-dual active set method for solving multi-rigid-body dynamic contact problems. Mathematics and Mechanics of Solids, 23(3), pp.489-503.

[47] Li, Y., Yuan, G. and Sheng, Z., 2018. An active-set algorithm for solving large-scale nonsmooth optimization models with box constraints. PloS one, 13(1), p.e0189290.

[48] Klaučo, M., Kalúz, M. and Kvasnica, M., 2019. Machine learning-based warm starting of active set methods in embedded model predictive control. *Engineering Applications of Artificial Intelligence*, *77*, pp.1-8.

[49] Raja, M.A.Z., Asma, K. and Aslam, M.S., 2018. Bio-inspired computational heuristics to study models of hiv infection of CD4+ T-cell. *International Journal of Biomathematics*, *11*(02), p.1850019.

[50] Parand, K., Kalantari, Z. and Delkhosh, M., 2018. Quasilinearization-Lagrangian method to solve the HIV infection model of CD4+ T cells. *SeMA Journal*, *75*(2), pp.271-283.

[51] Mirzaee, F. and Samadyar, N., 2019. On the Numerical Method for Solving a System of Nonlinear Fractional Ordinary Differential Equations Arising in HIV Infection of CD4 $$^{} $$ T Cells. *Iranian Journal of Science and Technology, Transactions A: Science*, *43*(3), pp.1127-1138.

[52] Yüzbaşı, Ş., 2016. An exponential collocation method for the solutions of the HIV infection model of CD4+ T cells. *International Journal of Biomathematics*, *9*(03), p.1650036.

[53] Atangana, A., Goufo, D. and Franc, E., 2014. Computational analysis of the model describing HIV infection of CD4. *BioMed research international*, *2014*.